Influence of polymer size on uptake and cytotoxicity of doxorubicin-loaded DNA–PEG conjugates

Laura Purdie, Cameron Alexander, Sebastian G. Spain[†,] and Johannes P. Magnusson**

School of Pharmacy, University of Nottingham, University Park, Nottingham, UK. NG7 2RD.

Oligonucleotides, Polymer, Physical prodrug, Drug Delivery

Intercalation of drugs into assembled DNA systems offers versatile new mechanisms for controlled drug delivery. However, current systems are becoming increasingly complex, reducing the practicality of large scale production. Here, we demonstrate a more pragmatic approach where a short DNA sequence was modified with poly[ethylene glycol] (PEG) of various lengths at both 5′-termini to provide serum stability and compatibility. The anti-cancer drug doxorubicin was physically loaded into two designed binding sites on the dsODN. The polymer conjugation improved the stability of the dsODN towards serum nucleases while its doxorubicin binding affinity was unaffected by the presence of the polymers. We examined the effects of polymer size on the dsODN carrier characteristics and studied the resulting DOX@DNA–PEG systems with respect to cytotoxicity, cellular uptake and localization in A549 and MCF7 cell lines. For the A549 cell line the DOX@DNA-PEG1900 exhibited the best dose response of the conjugates while DOX@DNA-PEG550 was the least potent. In MCF-7, a more doxorubicin sensitive cell line, all conjugates exhibited similar dose response to that of the free drug. Confocal microscopy analysis of doxorubicin localization shows that conjugates successfully deliver doxorubicin to the cell nucleus and also the lysosome. These data provide a valuable insight into the complexities of designing an oligonucleotide based drug delivery system and highlight some practical issues that need to be considered when doing so.

INTRODUCTION

In recent decades DNA-based materials have revolutionized the scope and complexity of nanomaterials that can be produced. Exploiting the specificity of Watson-Crick base pairing has produced complex dynamic structures such as molecular computers,(*1*) motors,(*2*) nanoreactors,(*3*) as well as sensors and diagnostics.(*4-10*) More recently, the ability of certain drugs to intercalate within the DNA double helix and form strong physical complexes has been utilized to form physical prodrugs for cytotoxics. Farokhzad et al. first demonstrated that a DNA aptamer could be loaded with doxorubicin (DOX), allowing targeted uptake into cells presenting the aptamer target.(*11*) This was extended to aptamer-targeted quantum dots(*12*) and polymer particles(*13*) allowing the addition of detection and delivery. Dabrowiak et al. have demonstrated several systems based upon gold nanoparticles (AuNPs) coated with DNA. Both DOX and actinomycin D (ActD) were intercalated into the helix, and targeting was achieved by introduction of folic acid onto one of the DNA strands.(*14-16*) "DNA origami" has also been used for intercalated delivery. Ahn et al. have demonstrated that a DNA tetrahedron, formed by annealing 4 strands, can be used to deliver DOX to cells, overcoming resistance in a multi-drug resistant cell line.(*17*) Leong et al. have used similar tetrahedra, decorated with AuNPs and loaded with ActD, for theranostic delivery to bacteria.(*18*) Högberg et al. have taken the origami approach a step further and designed large DNA bundles that can twist upon intercalation of DOX. Drug release kinetics, and thus cytotoxicity, can be modulated by varying the induced twist.(*19*)

Although these systems have demonstrated the feasibility of using DNA intercalation as a drug delivery mechanism, problems still remain. First, none have the shielding components required to prevent degradation and reduce potential immunogenic interactions in vivo, although some of the non-natural DNA conformations have been shown to be resistant to degradation.(*20*) Second, the systems being developed are displaying increasing complexity, in one case requiring over 200 short DNA

"staples" to hold the drug delivery system together, where each of which has to be synthesized and purified. PEG polymers have been extensively used to improve the pharmacokinetics of biologics.(*21*) Despite recent concerns about potential immunogenicity of PEG,(*22*) this remains controversial,(*23*) and they are still the polymer of choice for *in vivo* applications.

Herein we describe a more pragmatic approach to intercalating drug delivery. A simple, short, double stranded DNA was assembled from complementary oligonucleotides, modified with poly(ethylene glycol) (PEG) at the both 5′ positions. The effects of PEG polymer size on the ODN carrier delivery characteristics were examined. DOX was physically conjugated by intercalation into a pair of binding sites designed into the oligonucleotide sequence forming the DOX@DNA–PEG delivery system (Fig. 1).

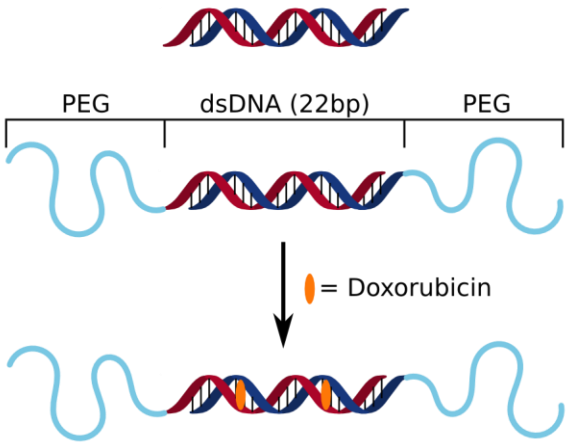

Figure 1. Schematic representation of intercalating DOX@DNA delivery system described herein.

RESULTS AND DISCUSSION

Synthesis and analysis of PEG-DNA conjugates.

PEG–DNA conjugates were synthesized in a similar manner to that described previously.(*10*) Polyethylene glycol monomethyl ether (mPEG, M_n 550, 1900 and 5000 Da) were activated with *N*,*N*-disuccinimidyl carbonate to form amino-reactive mPEG-succinimidyl carbonates (PEG-SC). The PEG-SCs were subsequently conjugated to 5′-aminohexyl modified single-stranded oligonucleotides to form a small library of PEG–ssDNA conjugates with 3 different PEG lengths, and consisting of two complementary DNA sequences (Oligo A: TAA CAG GAT TAG CAG AGC GAG G and Oligo B:

CCT CGC TCT GCT AAT CCT GTT A). Conjugates were purified by semi-preparative HPLC with typical isolated yields of 50–80% independent of mPEG length. HPLC and PAGE analysis (Fig. 2A and S1) confirmed no residual unmodified oligonucleotides in any of the conjugate samples. Molecular masses from MALDI-ToF mass spectrometry were generally in good agreement with theoretical values, however slight deviation from theoretical values was observed. This is not unexpected as mPEG is a disperse polymer and some molecular weight enrichment is likely to occur during HPLC purification i.e. polymer fractionation.

Lyophilized conjugates were dissolved in DNase-free annealing buffer and hybridized with the appropriate complementary strands (e.g. PEG550-A and PEG550-B) to form dsDNA conjugates with mPEG chains at both 5′-termini. Consequently, a series of three PEG DNA conjugates was produced, DNA–PEG550, DNA–PEG1900 and DNA–PEG5K, as well the unPEGylated, "unmodified" DNA. After annealing, the conjugates were analyzed by PAGE to ensure that no single stranded ODNs were remaining after the annealing (Fig. 2A and Fig S1A). PAGE analysis revealed that the PEG-ODNs had successfully formed the double stranded structures. Weak high molecular weight bands were observed for the single strands in all of the gels which arose from self-association of the unhybridized strands under the non-denaturing conditions.

Stability of DNA–PEG conjugates.

To determine the effect of PEG on DNA stability towards nucleases, DNA–PEG conjugates and unmodified DNA were incubated in presence of fetal calf serum. The conditions were chosen to mimic as closely as possible those used for later in vitro experiments to ensure that any effects that arose from differential degradation could be accounted for. The samples were analyzed by native PAGE and individual band intensity estimated using image analysis software. The band intensity of each conjugate at the start of the experiment (0 hours) was set as 100%. All DNA–PEG conjugates were stable for the duration of the experiment with 80–90% remaining after 72 h. Conversely, the unmodified DNA had completely degraded after 72 h and was reduced to approximately 40% after 48 h (Fig. 2B and S2). The conjugation of the PEG polymers to each terminus of the DNA therefore improved its stability

significantly and provided protection against the nucleases. However, no effect of polymer molecular weight on stability was observed under these conditions.

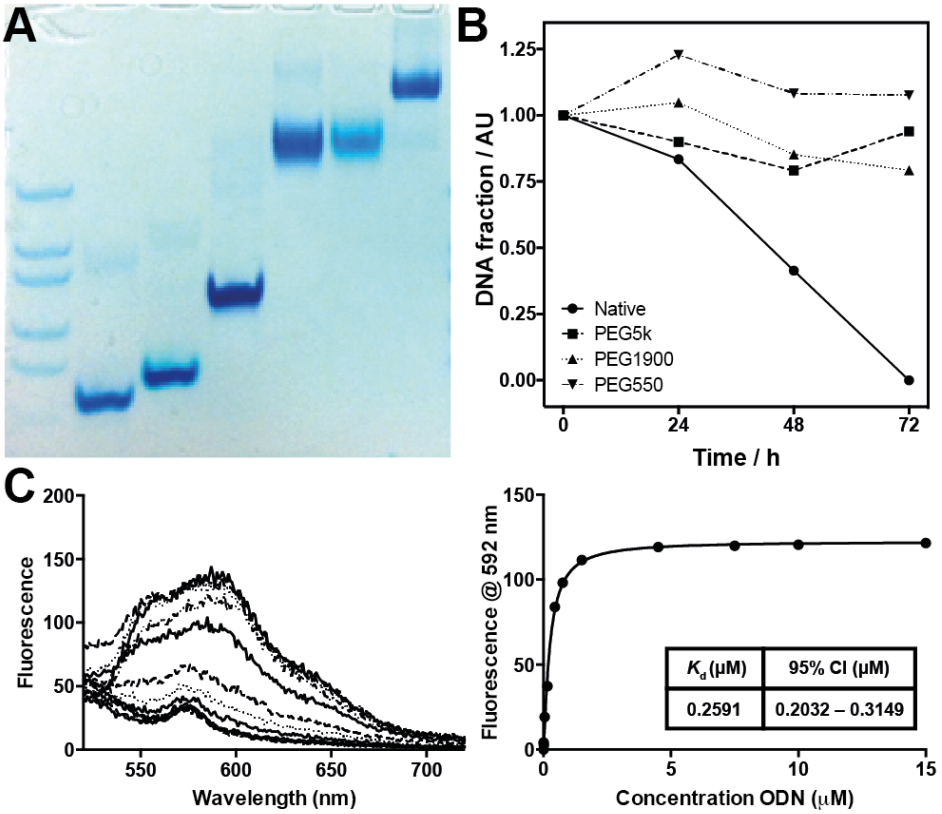

Figure 2. A. PAGE analysis of PEG5K-oligos and DNA–PEG5K conjugates. Lanes L-R: (1) IDT Ladder 10/60, (2) Oligo A, (3) Oligo B, (4) dsDNA, (5) PEG5K-A, (6) PEG5K-B, (7) DNA–PEG5K. B. Stability of DNA conjugates in serum. C. Affinity of doxorubicin for DNA–PEG1900 carriers. Fluorescence spectra of DOX with increasing ODN concentrations with corresponding Hill plots and calculated K_d values.

Doxorubicin-loading and affinity

The affinity of doxorubicin (DOX) to the DNA carriers was examined in order to determine the binding of the drug and if this was affected by PEGylation. Doxorubicin binds preferentially to 5′-GC-3′ and 5′-CG-3′ double stranded sequences,(*24*) thus it is expected that the sequence used here would have two preferential binding sites. Affinity measurements were performed by a previously established fluorescence quenching protocol.(*11*) The fluorescence of doxorubicin was plotted as a function of the oligonucleotide concentration to produce a Hill plot from which dissociation constants (K_d) were

calculated (Fig. 2C and S3). Comparison of the calculated K_d values showed no difference beyond experimental error between the PEGylated and non-PEGylated DNA, with all being 200 ± 60 nM.

In vitro cytotoxicity studies of DNA–PEG and DOX@DNA–PEG conjugates

DNA conjugates promote cell proliferation: To determine if the DNA–PEG conjugates were capable of delivering DOX they were assessed in vitro in A549 cells (lung adenocarcinoma epithelial cells). Carriers were loaded at a 1/10 (w/w) with DOX based on their oligonucleotide content (i.e. 1 mg DOX per 10 mg of ODN) forming the DOX@DNA–PEG conjugates. Cells were incubated with free DOX, DOX@DNA–PEG and empty DNA–PEG carriers for 72 h. DOX concentrations ranged from 0.15 nM–10 μM and were maintained across groups. For the unloaded conjugates the concentrations were matched to the oligonucleotide concentrations used in the DOX@DNA–PEG group. Metabolic activity was assessed by MTT assay, untreated cells were normalized as 100% metabolic activity.

As expected, free DOX resulted in complete suppression of metabolic activity at higher concentrations (≳1 μM), with a calculated IC50 of 89 nM (95% CI 57–131 nM, Fig. 3A). However, for DOX@DNA–PEG conjugates complete suppression was not seen even at very high concentrations of DOX (10 μM), with approximately 30% metabolic activity remaining compared to untreated cells (Fig. 3B and S3). Although intercalation of the DOX within a carrier is expected to affect cell entry, and thus cytotoxicity, this should be compensated for at the higher concentrations. When considered with the effect of the unloaded DNA–PEG (Fig. 3C) it is clear that the carriers alone promote metabolic activity/cell growth, and this promotion is also dose dependent. Visual inspection during the course of the experiment revealed that the cell density increased as a function of DNA concentration which was in an agreement with the MTT results. It has previously been shown that pyrimidine nucleosides are growth promoting when they are present in media at a concentration of 1μg/mL with endothelial cells. (22) Cells which are proliferating rapidly require a high rate of DNA synthesis. For those cells the rate of DNA synthesis can become the growth limiting factor. To administer 10 μM DOX, 58 μg/mL of the dsODN carrier was required. The proliferation of the A549 cell line was thus promoted by degradation

of the dsODN carrier and subsequent release of free nucleosides. The dsODN carrier was not shown to promote the proliferation of a MCF-7 breast cancer cell line.

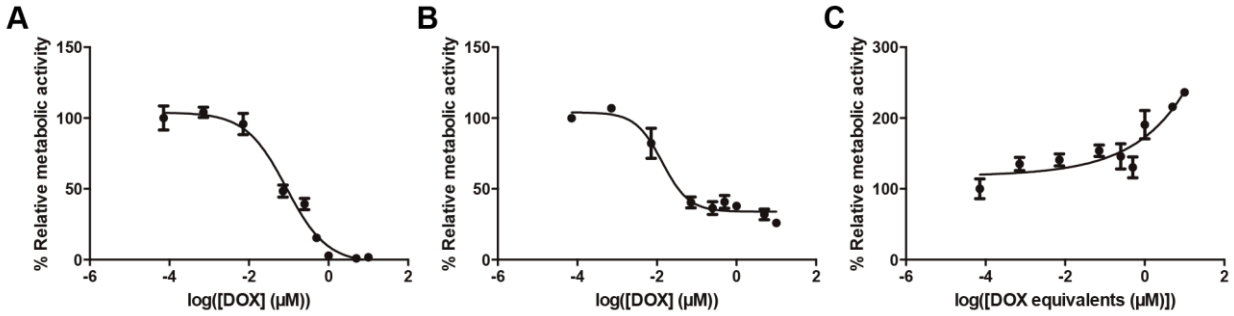

Figure 3. Cytotoxicity of A. doxorubicin; B. DOX@DNA–PEG1900; and C. DNA–PEG1900 dsODN in the A549 cell line.

Cytotoxicity of DOX@DNA–PEG and DNA–PEG. To counteract enhanced cell proliferation in the presence of oligonucleotide carriers further in vitro studies were performed in media supplemented with free nucleosides (A, C, G and T; 10 μg/mL each) for both cell lines. Cytotoxicity experiments were performed with A549 cells as before. With the addition of free nucleosides to the media no enhancement in cell proliferation was observed in the presence of unloaded dsODN carriers when compared to untreated cells (Fig. S4). For free DOX complete suppression of metabolic activity was observed at high concentrations as before (Fig 4). However, the calculated IC50 value increased to 124 nM (95% CI 102–151 nM) indicating that a higher dose of DOX is required to inhibit cell growth in the presence of nucleosides, further supporting our previous conclusions. The half maximal inhibitory concentration (IC50) is derived as the mid-point between the maximum and minimum of the dose response curve. However, since the maximal inhibition response varies between DOX@DNA carriers and to that of the free drug direct IC50 comparison between the groups was difficult. Consequently, IC50 values were also calculated by interpolation of the fitted curve at 50% viability. In the case of free DOX, where the maximum inhibition nears 100%, this has little effect on the calculated IC50 (126 nM c.f. 124 nM) however it provides a more realistic value for the DOX@DNA samples. Values calculated by both methods are contained with Table 1.

Table 1. Cytotoxicity data for doxorubicin and DOX@DNA complexes in A549 and MCF7 cells

Treatment	Cells	Curve Fit[a]		Interpolated[b]		
		IC50 (nM)[a]	95% CI (nM)	IC50 (nM)[a]	95% CI (nM)	$Vial_{max}$ (%±SD)[c]
DOX	A549	124	102–151	126	109–144	4.2±0.3
DOX@DNA	A549	67	43–104	132	104–165	19.3±2.0
DOX@DNA–PEG550	A549	167	105–265	541	411–718	30.8±7.0
DOX@DNA–PEG1900	A549	35	26–48	122	98–151	27.3±1.8
DOX@DNA–PEG5K	A549	66	47–92	232	189–282	28.0±1.9
DOX	MCF7	19	12–29	27	20–37	6.4±0.6
DOX@DNA	MCF7	31	19–52	37	27–49	3.4±0.5
DOX@DNA–PEG550	MCF7	32	21–50	40	31–50	9.8±1.2
DOX@DNA–PEG1900	MCF7	11	7–17	19	14–26	11.5±1.7
DOX@DNA–PEG5K	MCF7	10	8–15	17	13–24	4.2±0.3

[a] Calculated using the 4-parameter variable slope log(inhibitor) vs response model in Graphpad Prism 6.0. As incomplete inhibition was achieved for some treatments these values are relative to the achieved maximum inhibition. [b] Calculated by interpolation of the fitted curve at 50% relative metabolic activity. [c] Viability at maximum DOX concentration.

For non-PEGylated DOX@DNA, an IC50 of 132 nM (95% CI 104–165 nM) is comparable to that of free DOX. This is not unexpected considering that the unshielded DNA is readily degraded in the presence of serum and this is likely to be exacerbated in the presence of cells or if internalized. However, even at the highest non-PEGylated DOX@DNA concentration (1 μM) cell viability remains at ~20% compared to the untreated control. For the DOX@DNA–PEG samples IC50 values are strongly dependent on the molecular weight of the shielding polymer. DOX@DNA– PEG5K and DOX@DNA–PEG550, with IC50s of 232 nM (95% CI 189–282) and 541 nM (95% CI 411–718) respectively, are approximately 2- and 4-fold less toxic than DOX@DNA. DOX@DNA–PEG1900 maintains an IC50

similar to that of DOX@DNA and free drug with an IC50 of 122 nM (95% CI 98–151). The DOX@DNA–PEG conjugates all exhibited dose saturation at highest DOX@DNA concentrations and inhibition was limited to approximately 70% in comparison to 95% inhibition for the free drug.

In vitro studies were extended to a MCF7 cell line (breast adenocarcinoma epithelial cells) to determine if the limiting toxicity was cell line specific. MCF7 cells were more sensitive to DOX with an IC50 of 27 nM (95% CI 20–37) for free drug and all systems were capable of ~90–95% inhibition at the highest concentrations. The greater sensitivity results in less pronounced effects seen with polymer molecular weight, with little variation between treatments, particularly when the large confidence intervals are considered.

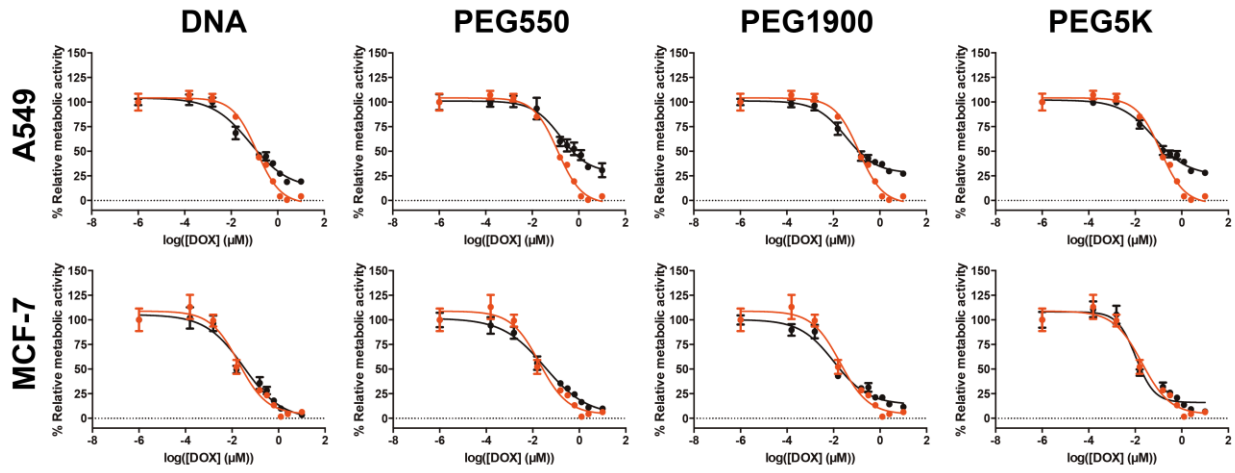

Figure 4. Cytotoxicity of DOX@DNA–PEG in A549 and MCF-7 cell lines. Cells were cultured in the presence of free nucleosides. Samples (black) are as labelled. Free DOX (red) is shown for comparison. Lines are calculated four-parameter logistic fits.

Confocal microscopy analysis of cells treated with DOX@DNA

DOX@DNA systems display cell line dependent localization. To further understand the cytotoxicity data DOX@DNA systems were studied by confocal microscopy in A549 and MCF7 cells. Cells were incubated with DOX@DNA carriers and free DOX and the localization studied at various time points using the inherent fluorescence of the drug for detection. Due to sensitivity requirements the drug concentration was fixed at 3 μM in all cases. After 3 hours (Fig. 5), free DOX showed intense staining in the nucleus in both cell lines indicating rapid uptake, while in all DOX@DNA nuclear

staining was considerably less intense. DOX@DNA samples contain punctate regions within the cytoplasm and in the perinuclear region; this was particularly pronounced in A549 cells. This demonstrates that dsODN are readily internalized into both A549 and MCF7 cells, albeit at lower levels than free drug, and allow trafficking into the target organelle. By 18 hours (Fig. 6) nuclear staining in MCF7 cells remains intense for both free drug and dsODN-DNA while other conjugates have lower levels. In contrast A549 cells have lower levels of nuclear staining compared to MCF7 cells but retain staining in cytoplasmic regions for all DOX@DNA samples and free DOX.

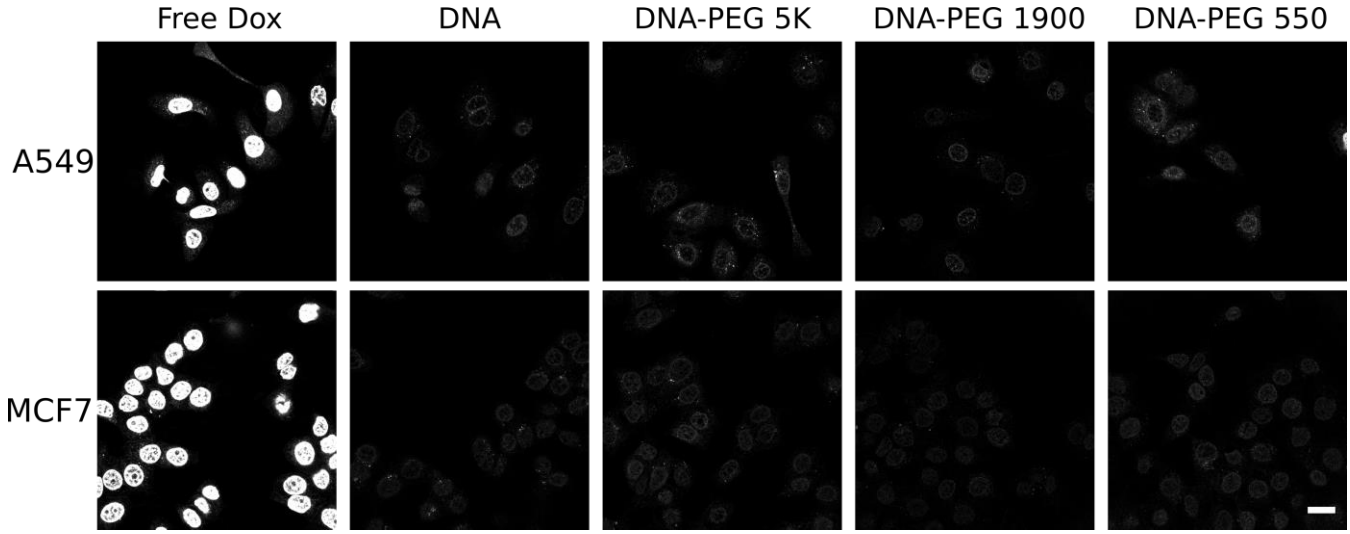

Figure 5. Cellular uptake DOX@DNA samples. Cells were incubated with doxorubicin loaded conjugates for 3 hours. Intrinsic doxorubicin fluorescence was visualized by confocal microscopy. Bar = 20 μm.

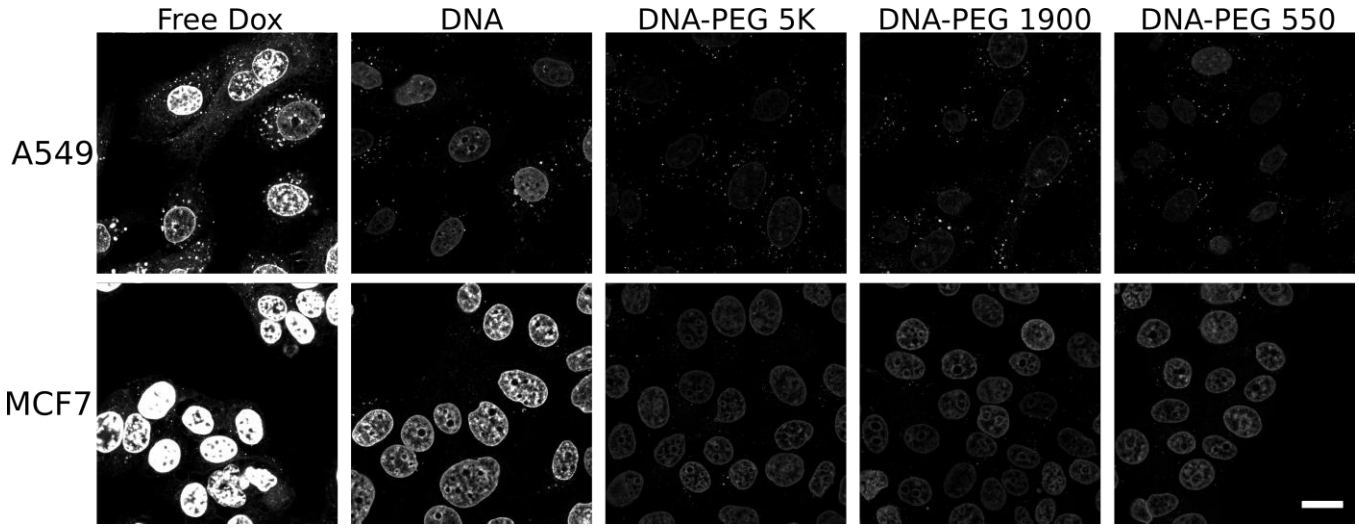

Figure 6. Cellular uptake DOX@DNA samples. Cells were incubated with doxorubicin loaded conjugates for 18 hours. Intrinsic doxorubicin fluorescence was visualized by confocal microscopy. Bar = 20 μm.

Intracellular localization after 18 hours

In order to investigate the intracellular localization of internalized DOX, cells were incubated for 18 hours with free DOX or DOX@DNA and the lysosomal compartments were counterstained (Fig. 7 and S6 for non-merged images). In MCF7 cells intense doxorubicin staining was observed in the nucleus for all dsODN and free dox. Furthermore, punctate doxorubicin positive regions co-localized with the lysosomal marker. In contrast, A549 cells showed no detectable nuclear staining at 18 hours, even for free DOX, while retaining cytoplasmic doxorubicin positive lysosomal staining. This contrasts with the findings of the previous experiment (Fig. 6) where some low level signal was still detected in nucleus of A549 cells at 18 hours. However, due to the broad excitation/emission spectra of both doxorubicin and the lysosomal marker, the collection range and signal gain for doxorubicin had to be narrowed to prevent signal bleed through. The co-localization assay (Fig. 7) therefore only visualized the most intense regions of doxorubicin staining i.e. the punctate cytoplasmic regions. Lower levels of doxorubicin fluorescence may reflect increased efflux of doxorubicin from A549 cell nuclei in comparison to MCF7 cells which could explain the cell lines elevated resistance to the drug. Both cell lines have been shown to express multidrug resistance associated-proteins (MRP) which can limit the efficiency of chemotherapy.(*25*) Encapsulation of doxorubicin in dsODN allows the drug to traffic into the nucleus and lysosome however it does not alter the final destination of the doxorubicin nor prevent drug efflux. However, replacement of the oligonucleotide segment with one that exerts its own therapeutic effect, e.g. siRNA or T-oligos,(*26, 27*) may provide a synergistic effect.

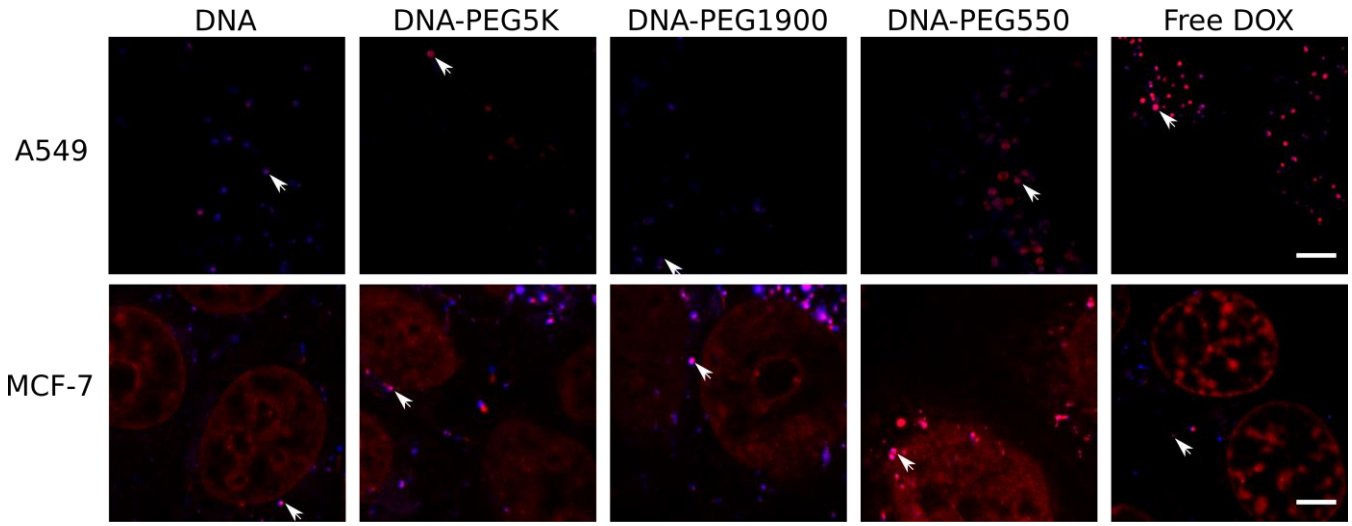

Figure 7. Doxorubicin co-localizes with a lysosomal marker. MCF-7 and A549 cells were incubated with DOX@DNA-PEG for 18 hours then counterstained for lysosomes with CytoPainter Lysosome Blue. Doxorubicin (red) and lysosomal (blue) staining was visualized by confocal microscopy. Arrows: areas of colocalization. Bar = 5 μm

CONCLUSIONS

We have described the synthesis and in vitro biological activity of a series of oligonucleotide-based carriers for doxorubicin. Carriers were synthesized by conjugation of PEG to the 5' termini of ODN and hybridization by Watson-Crick base pairing. As expected, PEGylation was found to enhance stability to serum nucleases compared to an unPEGylated control. DOX was successfully bound to the carriers with high affinity (K_d ~200 nM) in all cases.

Initial in vitro assays with A549 cells revealed that the carriers promoted cell growth compared to untreated control, with later experiments requiring supplementation with free nucleosides to enable comparison. Comparisons of the metabolic activity, uptake and localization of DOX@DNA systems in A549 and MCF7 cells demonstrated several differences. In MCF7 cells, metabolic activity and uptake were comparable to that of free DOX. Conversely, in A549 cell line DOX@DNA systems had a lesser effect on metabolic activity than free DOX with no

system able to achieve more than 70% inhibition. Uptake studies determined that DOX@DNA systems were taken up to a lower extent than free DOX, and that DOX levels in nuclei reduced with time in A549 cells compared to MCF7 cells

Our findings highlight the issues that need to be addressed when designing and evaluating oligonucleotide based drug delivery systems. The vast difference observed between the two cell lines underlines the importance of adopting appropriate in vitro models early on and supplementing tissue culture medium with free nucleosides. Our results suggest that our PEG-based system could be used to treat doxorubicin sensitive cancer cells in instances where adverse drug effects are limiting. The data derived from A549 cell line also accentuates the fact that PEGylated-dsODN system would be not suitable to treat drug resistance cells, in those circumstances amphiphilic polymers and known inhibitors of multidrug resistance protein (MRP) should be considered instead.(*28, 29*) We are currently evaluating alternative dsODN-derived systems to address this issue of drug resistance.

MATERIALS AND METHODS

Materials

All oligonucleotides (HPLC purified) were purchased from Biomers.net GmbH (Ulm, Germany) and used without further purification. MCF-7 and A549 cell lines were received from CRN NCI-60 cell bank.

Polyethylene glycol monomethyl ether (mPEG, M_n 5000, 1900 and 550 Da) were purchased from Polysciences Inc. CytoPainter lysosomal staining kit blue fluorescence was purchased from Abcam. *N*,*N*′-Disuccinimidyl carbonate (DSC, ≥95.0%), triethylamine (Et_3N, ≥99%), thiazolyl blue tetrazolium bromide (MTT, 98%), water (BPC grade), diammonium hydrogen citrate (DAHC, ≥99%), Stains-All (95%), 3-hydroxypicolinic acid (3-HPA, (≥99%)), methylene blue

hydrate (>97%), tris-borate-EDTA buffer (TBE, 10× concentrate), ammonium persulfate (≥98%), *N*,*N*,*N*′,*N*′-tetramethylethylenediamine (TEMED, 99%), ethylenediaminetetraacetic acid disodium salt (EDTA, >99%), glycerol anhydrous (Fluka), bromophenol blue solution (0.04 wt% H_2O), acrylamide:*N*,*N*′-methylenebisacrylamide (29:1) 40% solution and Dulbecco's PBS (Modified, without calcium chloride and magnesium chloride) were purchased from Sigma Aldrich.

All other solvents and reagents were of analytical or HPLC grade and purchased from Sigma Aldrich unless otherwise specified.

NMR Spectroscopy

NMR spectra were recorded on a Bruker Avance 400 spectrometer at 400.13 MHz (^{1}H) and 100.62 MHz (^{13}C, ^{1}H decoupled at 400.13 MHz) in chloroform-d. All chemical shifts are reported in ppm relative to the signal for tetramethylsilane.

HPLC analysis and purification of DNA strands

Reverse phase high performance liquid chromatography (RP-HPLC) was performed on a Shimadzu Prominence UPLC system fitted with a DGU-20A5 degasser, LC-20AD low-pressure gradient pump, CBM-20A LITE system controller, SIL-20A autosampler and an SPD-M20A diode array detector. Analytical separations were performed on a Phenomenex Clarity 3 μm Oligo-RP C18 column (4.6×50 mm) with a gradient of MeOH (10–70% for PEG5K and PEG1900 ODNs and 10–50% for PEG550 ODNs over 20 min) in 0.1 M triethylammonium acetate (TEAA, pH 7.5)/MeCN (95/5) as the mobile phase at a flow rate of 1.0 mL/min. Semi-preparative separations were performed on a Phenomenex Clarity 3 μm Oligo-RP C18 column (10×50 mm) under the same conditions at a flow rate of 5.0 mL/min.

MALDI-ToF Mass Spectrometry

Matrix-assisted laser desorption/ionization time-of flight (MALDI-ToF) mass spectrometry was performed on a Bruker MALDI-ToF Ultra Flex III spectrometer operated in linear, positive ion mode. 3-HPA containing DAHC was used as the matrix for oligonucleotide analysis. Briefly, a saturated solution of 3-HPA (50 mg/mL) was prepared by adding 25 μg of 3-HPA to 500 μL of 50% MeCN/water. 25 μL of DAHC solution (100 mg/mL) was added to 225 μL of the 3-HPA solution, to give a final DAHC concentration of 10 mg/mL. ODN solutions were desalted prior to mixing with matrix using C18 Ziptips. Equal volumes of matrix solution and ODN solution (0.2 mM) were mixed and 2 μL of the mixture was spotted onto the MALDI plate and allowed to dry.

Polyacrylamide Gel Electrophoresis

Polyacrylamide gel electrophoresis (PAGE) analysis was performed at 160 mV using a 15% acrylamide running gel. Native gels were prepared using acrylamide–bis-acrylamide (29:1) and TBE (Tris-borate-EDTA) solutions. Samples were prepared by dilution in native loading buffer containing glycerol and bromophenol blue. 5 μg of oligonucleotide was loaded per well. IDT Oligo Length Standard 10/60 was used a size marker for the gels. The oligonucleotide/polymer bands were visualized using methylene blue staining.

Synthesis of α-methoxy-ω-succinimidyl carbonate poly[ethylene glycol] (mPEG-SC)

mPEG550-SC. mPEG (M_n 550 Da, 1.39 g, 2.5 mmol) was dried by azeotropic distillation with toluene. The residue was dissolved in THF (100 mL) and the solution cooled to 0°C with an ice bath. DSC (1.89 g, 7.4 mmol) and TEA (0.745 g, 7.4 mmol) were added and the solution allowed to warm to room temperature then stirred overnight (16 h). The resulting suspension was filtered and volatiles removed under reduced pressure. The residue was dissolved in toluene and any insoluble material removed by filtration. Toluene was removed under reduced pressure and the

residue redissolved in chloroform. In order to remove any unreacted DSC Wang resin/TEA was added to the solution and allowed to react overnight. The resin was removed by centrifugation and the supernatant was washed with 0.1 M HCl. The organic layer was dried over MgSO4, filtered and volatiles removed under reduced pressure. The product was dried under vacuum and isolated as yellowish oil (400 mg, 20% yield).

^{1}H NMR (CDCl3, 400 MHz): δ 4.49–4.47 (t, 2H), 3.82–3.56 (m, 50H), 3.40 (s, 3H), 2.86 (s, 4H).

mPEG1900-SC. mPEG (M_n 1900 Da, 3g, 1.6 mmol) was dried by azeotropic distillation with toluene. The residue was dissolved in MeCN (70 mL) and the solution cooled to 0 °C with an ice bath. DSC (1.01 g, 4 mmol) and TEA (0.4 g, 4 mmol) were added and the solution allowed to warm to room temperature then stirred overnight (16 h). The resulting suspension was filtered and concentrated under reduced pressure. The crude product was precipitated into Et2O and collected by vacuum filtration. The product was purified by twice re-dissolving in $CHCl_3$ and precipitating into Et_2O. After drying under vacuum the product was recovered as white powder (1.5 g, 47% yield).

^{1}H NMR ($CDCl_3$, 400 MHz): δ 4.49–4.47 (t, 2H), 3.84–3.48 (m, 206H), 3.40 (s, 3H), 2.86 (s, 4H).

mPEG5000-SC. mPEG5000-SC was synthesized by the same protocol as mPEG1900-SC starting for mPEG (M_n 5 kDa). Isolated 7 g, 68% yield.

^{1}H NMR ($CDCl_3$, 400 MHz): δ 4.49–4.47 (t, 2H), 3.85–3.48 (m, 522H), 3.40 (s, 3H), 2.86 (s, 4H).

General procedure for the synthesis of PEGylated oligonucleotides

PEGylated oligonucleotides were synthesized as previously described.(*10*) Specific reaction conditions are detailed in table 2. Briefly, 5′-aminohexyl oligonucleotide (1 eq.) was dissolved in DPBS to a concentration of 2.5 mg/mL. A solution of mPEG-SC (5 eq.) was added with gentle agitation and the reaction allowed to proceed for up to 72 h. Conversion was monitored by HPLC and additional mPEG-SC added if required. PEGylated oligonucleotides were purified by semi-preparative HPLC and lyophilized. Lyophilized materials were redissolved in DNase free water and concentration determined by measurement of optical density at 260 nm (1 OD = 20 μg/mL). Solutions were then aliquoted and lyophilized before storage at -20 °C.

Table 2. Conditions and analytical data for the PEGylation of oligonucleotides

Oligo[a]	PEG	Equiv.	Solvent[b]	Yield[c]	MALDI[d]
A	550	5	THF	66	7729/7633
B	550	5	THF	54	7484/7386
A	1900	5	DMSO	75	9079/9076
B	1900	5	THF	56	8834/9271
A	5000	5	DMSO	54	12189/12189
B	5000	6.7	DMSO	84	11934/12006

[a] Sequences. Oligo A: TAA CAG GAT TAG CAG AGC GAG G; Oligo B: CCT CGC TCT GCT AAT CCT GTT A. [b] for dissolution of mPEG-SC. [c] calculated from measured OD values. [d] theoretical/found.

Hybridization of DNA strands

Strands were hybridized in annealing buffer which consisted of 10 mM Tris, 50 mM NaCl and 1 mM EDTA pH 7.5. For the hybridisation the strands were mixed in equimolar quantities to give a final concentration of 75 μM of each strand and placed in a water bath at 95 °C for 5 minutes. The water bath was then turned off and allowed to cool slowly to room temperature.

Annealed strands were desalted using a PD SpinTrap G-25 column (GE Healthcare) and oligonucleotide concentration determined by optical density @ 260 nm (1 OD = 30 ug/mL). Annealing was verified using PAGE gel under non-denaturing conditions. Solutions were aliquoted, lyophilized and stored at -20 °C until needed.

Drug loading of DNA carriers

Doxorubicin HCl (Dox HCl) (1 mg) was dissolved in UHQ water (1 mL). The solution was filtered through a 0.22 μm PES syringe filter and stored at 4 °C until use. DNA carriers were dissolved in sterile DPBS. Dox HCl was added to the DNA solution in order to achieve a 10% (w/w) Dox HCl to DNA drug loading. The DOX@DNA complexes were allowed to form for 30 min. and used without further purification. For in vitro experiments the DOX@DNA complexes were diluted 25-fold with media to a DOX concentration of 10 μM (5.8 μg/mL of DOX, 58 μg/mL ODN).

Stability of oligonucleotides

DOX@DNA systems were incubated at an oligonucleotide concentration of 0.63 μg/mL in DPBS containing 10% Fetal Calf Serum (FCS). Solutions were incubated at 37 °C with mild agitation. At each time point (0, 24, 48, 72 h) a sample (10 μL) was removed, flash frozen in liq. N_2, and stored at -20 °C until analysis by PAGE. The samples were diluted with 10 μL of loading buffer and 10 μL of the diluted sample loaded per well. PAGE was carried out at 160 mV using a 15% acrylamide gel. The oligonucleotide/polymer bands were visualized using methylene blue. Intensity of gel bands was estimated by image analysis using Scion Image (Macro: Gelplot2).

Affinity of doxorubicin HCl to hybridized oligonucleotide strands

A fluorescence spectroscopy method(*11*) was used to assess the binding affinity of DOX for DNA systems. The assay was performed with a constant DOX concentration (1.5 μM) while DNA carrier was titrated from 0 to 15 molar (DNA concentrations: 15, 10, 7.5, 4.5, 1.5, 0.75, 0.45, 0.15, 0.045 , 0.015, 0.005 and 0 μM). A Hill plot was used to determine the binding affinity of the double stranded oligonucleotide sequence to doxorubicin HCl (Y: (F0-F), X: Concentration ODN μM). All analyses were performed in Graphpad Prism 6.0.

In vitro assays

General. The MCF-7 cells were grown in standard T75 flasks. A549 cells were grown in T75 flasks treated for optimal attachment (Corning T75 Cat no 430641). Both cell lines were grown in Minimum Essential Medium Eagle (MEM) media containing 4 mM L-Glutamine, Penicillin/Streptomycin and 10 % FCS. The media was supplemented with nucleosides (G, C, T, A) at the later stages of the cell work, each nucleoside was added at a final concentration of 10 μg/L.

Cytotoxicity Assays. Cells were allowed to reach confluence in the T75 flasks before being seeded onto 96-well plates. Cells were seeded at 5×10^3 cells/well for both cell lines (100 μL, 5×10^4 cells/mL). Cells were allowed to attach for 24 hours before the media was removed and replaced with 100 μL of media containing the appropriate DOX concentration. For experiments with carrier alone, an equivalent concentration of DNA (without drug) was used. 6 wells were used for each concentration. Cells were treated for 72 hours before metabolic activity was determined using an MTT assay. MTT solution (10 μL of 5 mg/mL) in media was added to each well and allowed to develop for 75 minutes. The media was then carefully aspirated and wells washed with PBS (100 μL). The formazan crystals were finally dissolved by adding DMSO (100 μL) to each well. The plate was read using a Tecan M200 platereader at 562 nm and the MTT

response compared to untreated cells. Untreated cells were normalized as 100% metabolic activity.

Toxicity curves were fitted with Graphpad Prism 6.0 using the 4-parameter variable slope log(inhibitor) vs response model. Due to incomplete inhibition IC50 calculated are considered as relative. Real IC50 values were calculated by interpolation of the fitted curve within the same software.

Confocal Microscopy

Cells were seeded on Nunc LabTekII coverglass 8 well slides at 20,000 cells/well and incubated overnight. Conjugates were loaded with drug as described above and added to cells at a final doxorubicin concentration of 3μM. After the required incubation time cells were fixed in cold 4 % paraformalydehyde in PBS for 10 minutes. Samples were stored at 4 °C and imaged by Laser Scanning Confocal Microscopy (LSCM) within 24 hours. Settings were excitation 532 nm laser, emission 552-654 nm. Lysosomal staining was conducted using CytoPainter Lysosomal staining kit – blue (Abcam, ab112135) following the manufacturer's instructions with an incubation time of 20 minutes. Cells were imaged immediately by LSCM using settings excitation 405 nm, emission 430-480 nm and excitation 532 nm, emission 553-672.

ACKNOWLEDGEMENTS

The authors thank Christine Grainger-Boultby, Tom Booth and Paul Cooling for technical support.

FUNDING

All work was funded by the UK EPSRC (Grants EP/H005625/1, EP/G042462/1) awarded to CA.

SUPPORTING INFORMATION

PAGE analysis of annealed strands and degradation study. HPLC traces of purified PEG-ODN conjugates. Doxorubicin-ODN affinity plots. MTT cytotoxicity assays in absence of nucleosides and doxorubicin (ODN-carrier only). Additional colocalization images. This material is available free of charge via the Internet at http://pubs.acs.org.

AUTHOR INFORMATION

Corresponding Author

*Email: johannespall@gmail.com, s.g.spain@sheffield.ac.uk.

Present Addresses

† Department of Chemistry, University of Sheffield, Brook Hill, Sheffield. S3 7HF. UK.

Author Contributions

LP, SGS and JPM performed experiments. All authors contributed to experimental design. The manuscript was written through contributions of all authors. All authors have given approval to the final version of the manuscript.

ABBREVIATIONS

PEG, Polyethylene glycol; DOX, Doxorubicin; DNA, Deoxyribonucleic acid; ODN, Oligonucleotide; dsODN, Double stranded oligonucleotide; DOX@DNA-PEG, Pegylated double stranded oligonucleotide physically complexed with doxorubicin; DOX@DNA, Double stranded oligonucleotide physically complexed with doxorubicin; IC, Inhibitory concentration; CI, Confidence interval; MTT, Thiazolyl Blue Tetrazolium Blue; HPLC, High performance liquid chromatography; MALDI-ToF, Matrix-assisted laser desorption/ionization time-of flight mass spectroscopy; NMR, Nuclear magnetic resonance; PAGE, Polyacrylamide gel electrophoresis.

REFERENCES

(1) Chakraborty, B., Jonoska, N., and Seeman, N. C. (2012) A programmable transducer self-assembled from DNA. *Chem. Sci. 3*, 168-176.

(2) Bath, J., Green, S. J., and Turberfield, A. J. (2005) A free-running DNA motor powered by a nicking enzyme. *Angew. Chem. Int. Ed. 44*, 4358-4361.

(3) McKee, M. L., Milnes, P. J., Bath, J., Stulz, E., Turberfield, A. J., and O'Reilly, R. K. (2010) Multistep DNA-Templated Reactions for the Synthesis of Functional Sequence Controlled Oligomers. *Angew. Chem. Int. Ed. 49*, 7948-7951.

(4) Roh, Y. H., Lee, J. B., Kiatwuthinon, P., Hartman, M. R., Cha, J. J., Um, S. H., Muller, D. A., and Luo, D. (2011) DNAsomes: Multifunctional DNA-Based Nanocarriers. *Small 7*, 74-78.

(5) Roh, Y. H., Ruiz, R. C. H., Peng, S., Lee, J. B., and Luo, D. (2011) Engineering DNA-based functional materials. *Chem. Soc. Rev. 40*, 5730-5744.

(6) Chien, M.-P., Thompson, M. P., and Gianneschi, N. C. (2011) DNA-nanoparticle micelles as supramolecular fluorogenic substrates enabling catalytic signal amplification and detection by DNAzyme probes. *Chem. Commun. 47*, 167-169.

(7) Chien, M.-P., Rush, A. M., Thompson, M. P., and Gianneschi, N. C. (2010) Programmable Shape-Shifting Micelles. *Angew. Chem. Int. Ed. 49*, 5076-5080.

(8) Cutler, J. I., Auyeung, E., and Mirkin, C. A. (2012) Spherical Nucleic Acids. *J. Am. Chem. Soc. 134*, 1376-1391.

(9) Cutler, J. I., Zhang, K., Zheng, D., Auyeung, E., Prigodich, A. E., and Mirkin, C. A. (2011) Polyvalent Nucleic Acid Nanostructures. *J. Am. Chem. Soc. 133*, 9254-9257.

(10) Magnusson, J. P., Fernandez-Trillo, F., Sicilia, G., Spain, S. G., and Alexander, C. (2014) Programmed assembly of polymer-DNA conjugate nanoparticles with optical readout and sequence-specific activation of biorecognition. *Nanoscale 6*, 2368-74.

(11) Bagalkot, V., Farokhzad, O. C., Langer, R., and Jon, S. (2006) An aptamer-doxorubicin physical conjugate as a novel targeted drug-delivery platform. *Angew. Chem. Int. Ed. 45*, 8149-8152.

(12) Bagalkot, V., Zhang, L., Levy-Nissenbaum, E., Jon, S., Kantoff, P. W., Langer, R., and Farokhzad, O. C. (2007) Quantum Dot−Aptamer Conjugates for Synchronous Cancer Imaging, Therapy, and Sensing of Drug Delivery Based on Bi-Fluorescence Resonance Energy Transfer. *Nano Lett. 7*, 3065-3070.

(13) Zhang, L., Radovic-Moreno, A. F., Alexis, F., Gu, F. X., Basto, P. A., Bagalkot, V., Jon, S., Langer, R. S., and Farokhzad, O. C. (2007) Co-Delivery of Hydrophobic and Hydrophilic Drugs from Nanoparticle–Aptamer Bioconjugates. *ChemMedChem 2*, 1268-1271.

(14) Alexander, C. M., Maye, M. M., and Dabrowiak, J. C. (2011) DNA-capped nanoparticles designed for doxorubicin drug delivery. *Chem. Commun. 47*, 3418-3420.

(15) Alexander, C. M., Dabrowiak, J. C., and Maye, M. M. (2012) Investigation of the drug binding properties and cytotoxicity of DNA-capped nanoparticles designed as delivery vehicles for the anticancer agents doxorubicin and actinomycin D. *Bioconjugate Chem. 23*, 2061-70.

(16) Alexander, C. M., Hamner, K. L., Maye, M. M., and Dabrowiak, J. C. (2014) Multifunctional DNA-Gold Nanoparticles for Targeted Doxorubicin Delivery. *Bioconjugate Chem. 25*, 1261-1271.

(17) Kim, K. R., Kim, D. R., Lee, T., Yhee, J. Y., Kim, B. S., Kwon, I. C., and Ahn, D. R. (2013) Drug delivery by a self-assembled DNA tetrahedron for overcoming drug resistance in breast cancer cells. *Chem. Commun. 49*, 2010-2.

(18) Setyawati, M. I., Kutty, R. V., Tay, C. Y., Yuan, X., Xie, J., and Leong, D. T. (2014) Novel Theranostic DNA Nanoscaffolds for the Simultaneous Detection and Killing of Escherichia coli and Staphylococcus aureus. *ACS Appl. Mater. Interfaces*.

(19) Zhao, Y.-X., Shaw, A., Zeng, X., Benson, E., Nyström, A. M., and Högberg, B. (2012) DNA Origami Delivery System for Cancer Therapy with Tunable Release Properties. *ACS Nano 6*, 8684-8691.

(20) Seferos, D. S., Prigodich, A. E., Giljohann, D. A., Patel, P. C., and Mirkin, C. A. (2009) Polyvalent DNA nanoparticle conjugates stabilize nucleic acids. *Nano Lett. 9*, 308-11.

(21) Duncan, R. (2003) The dawning era of polymer therapeutics. *Nat. Rev. Drug Discov. 2*, 347-360.

(22) Knop, K., Hoogenboom, R., Fischer, D., and Schubert, U. S. (2010) Poly(ethylene glycol) in Drug Delivery: Pros and Cons as Well as Potential Alternatives. *Angew. Chem. Int. Ed. 49*, 6288-6308.

(23) Schellekens, H., Hennink, W. E., and Brinks, V. (2013) The Immunogenicity of Polyethylene Glycol: Facts and Fiction. *Pharm. Res. 30*, 1729-1734.

(24) Frederick, C. A., Williams, L. D., Ughetto, G., Vandermarel, G. A., Vanboom, J. H., Rich, A., and Wang, A. H. J. (1990) Structural comparison of anticancer drug DNA complexes - adriamycin and daunomycin. *Biochemistry 29*, 2538-2549.

(25) Abdallah, H. M., Al-Abd, A. M., El-Dine, R. S., and El-Halawany, A. M. (2015) P-glycoprotein inhibitors of natural origin as potential tumor chemo-sensitizers: A review. *J. Adv. Res. 6*, 45-62.

(26) Sarkar, S., and Faller, D. V. (2011) T-Oligos Inhibit Growth and Induce Apoptosis in Human Ovarian Cancer Cells. *Oligonucleotides 21*, 47-53.

(27) Resnier, P., Montier, T., Mathieu, V., Benoit, J.-P., and Passirani, C. (2013) A review of the current status of siRNA nanomedicines in the treatment of cancer. *Biomaterials 34*, 6429-6443.

(28) Batrakova, E. V., Dorodnych, T. Y., Klinskii, E. Y., Kliushnenkova, E. N., Shemchukova, O. B., Goncharova, O. N., Arjakov, S. A., Alakhov, V. Y., and Kabanov, A. V. (1996) Anthracycline antibiotics non-covalently incorporated into the block copolymer micelles: in vivo evaluation of anti-cancer activity. *Br. J. Cancer 74*, 1545-1552.

(29) Guo, Y., Luo, J., Tan, S., Otieno, B. O., and Zhang, Z. (2013) The applications of Vitamin E TPGS in drug delivery. *Eur. J. Pharm. Sci. 49*, 175-186.

For table of contents only